2014 Canada-China Conference on Advanced Reactor Development (CCCARD-2014)
Niagara Falls Marriott Fallsview Hotel & Spa, Niagara Falls, Ontario Canada, April 27-30, 2014.

CCCARD2014-069

EFFECT OF MICROSTRUCTURE ON HIGH TEMPERATURE MECHANICAL PROPERTIES AND RADIATION DAMAGE IN ZR ALLOY EXCEL

Y. Idrees[1], M. Sattari[1,2], Z. Yao[1], M.R. Daymond[1]
[1]Dept. of Mechanical and Materials Engineering, Queen's University, Kingston, ON, Canada, K7L 3N6
[2]Dept. of Chemical and Biological Engineering, Division of Energy and Materials, Chalmers University of Technology, Sweden

Abstract

The present paper reviews recent work on the effect of microstructure on the mechanical behavior, creep behavior and stability under irradiation of Zr alloy Excel. A series of heat treatments were performed on Excel to achieve different microstructures. High temperature tensile tests, creep-rupture tests and heavy ion irradiation experiments were performed on selected microstructures. Formation of <c>-component loops and decomposition of β_{Zr} has been studied. Furthermore, suggestions have been made regarding the microstructural stability.

1 Introduction

The Canadian CANDU-Super Critical Water-Cooled Reactor (SCWR) is one Generation-IV reactor design [1]. The need to increase thermal efficiency requires increased operating temperatures and pressures, beyond that of the existing CANDU design. The CANDU-SCWR is designed to have a maximum coolant temperature and pressure of 625°C and 25 MPa respectively, compared to 310°C and 10 MPa in current CANDU reactors. Hence the standard CANDU pressure tube design and material cannot be used for the CANDU-SCWR [2]. Two possible designs for the fuel channel have been proposed: the high efficiency channel (HEC) design and the re-entrant channel (REC) design. In the HEC design, each pressure tube operates at an average temperature of about 80°C, whereas in the REC design, the pressure tube operates at a temperature of about 350°C to 400°C. According to several studies on developing creep-resistant alloys for pressure tubes it was found that a composition in the range 3-4% Sn- 0.5-1.5% Mo- 0.5-1.5% Nb gives promising creep properties and higher strength with low neutron capture cross-section [3,4,5]. Therefore, for both the HEC and REC designs, a high strength and creep resistant zirconium-alloy Excel developed by AECL [5,6,7] was chosen as the reference material. The microstructure of Excel differs from common Zr alloys such as Zircaloy-2, 4, and Zr-2.5% Nb due to different chemical compositions; however, there are some similarities between the α-phase of Zr-Excel alloy and the Zircaloys due to the presence of tin as a solute. The alloy also resembles Zr-2.5%Nb in the sense of possessing a dual phase microstructure, and the presence of Nb in the β-phase [8].

Previous experience of Zr based alloys as reactor-core components have demonstrated the severe challenges faced during service. The challenges include but are not limited to: irradiation growth, irradiation and thermal creep, degradation of mechanical properties and plastic instability. Several past studies have shown that Excel exhibits superior or comparable mechanical,

properties and creep resistance compared to Zr-2.5Nb. It has been found that under the same metallurgical conditions, Excel has higher tensile strength than Zr-2.5Nb [6]. Furthermore, in the extruded and stress relieved condition, as well as extruded and cold drawn condition, Excel shows lower creep rates than cold worked Zr-2.5% Nb [4]. Another study by Cheadle et al. [6] showed lower creep rates for Excel in all metallurgical conditions, as compared to Zr-2.5%Nb in the same condition. Furthermore, the creep rates of 5% cold-worked and annealed Excel, derived from stress relaxation rates after 4000 hr at 297°C under 100 MPa stress and a neutron flux of 2×10^{17} $n.m^{-2}.s^{-1}$, were found to be a half and a third respectively of that observed for Zr-2.5% Nb tubes under similar metallurgical conditions. It was found that the difference between axial and transverse creep rates was comparable to that seen for Zr-2.5% Nb with a similar texture, which suggests a similar creep anisotropy in the two alloys. In an experimental study, Tucker et al. [9] have shown that irradiation growth in Excel is both fluence and temperature dependent. At high neutron fluences ($5\text{-}15\times10^{25}$ $n.m^{-2}$) and temperatures above 376°C, Excel suffers higher growth strains than other Zr based alloys under similar irradiation conditions. However, at lower temperatures, the growth in Excel was found to be comparable to that in Zircaloy-4. This variation in the growth strains between Excel and other Zr based alloys has been attributed to the fact that for these alloys the microstructure and its evolution during irradiation differs. It has been established that vacancy type basal plane <c>-component loops are formed during neutron irradiation of Zr at temperatures close to $0.3T_m$ [10,11,12]. Irradiation growth is strongly affected by the microstructure and microchemistry of Zr alloys. Regarding the microstructural evolution in Excel, a limited data has been presented so far, demanding further irradiation studies [13].

Recent work at Queen's has investigated several heat treatments in order to modify the Excel microstructure. Mechanical properties of selected microstructures have been assessed and compared. The high temperature tensile properties of Excel pressure tube material are reported here as a function of microstructure, along with stress-rupture tests providing preliminary investigations into the effect on creep properties. Secondly, in-situ heavy-ion irradiation experiments were conducted on several microstructures, to study the microstructural stability of selected Excel microstructures. The major focus of the irradiation experiments were the formation of <c>-component loops, decomposition of beta phase and irradiation induced microchemical changes.

2 Materials and Methods

The material used in this study is an Excel alloy pressure tube, a material consisting of α Zr-hcp and β Zr-bcc phases, with the specified chemical composition of Zr- 3.5 wt.% Sn- 0.8 wt.% Mo- 0.8 wt.% Nb- 0.2 wt.% Fe. The tube, provided by AECL Chalk River Nuclear Laboratories, is designated XL 601. The tube was made by extruding a hollow billet preheated to 850°C at a ratio of 10:1 followed by 25% cold drawing. The tube was then annealed at 750°C for 30 minutes and stress relieved at 400°C for 24 hours. A number of experimental techniques used have been described below:

2.1 Heat treatments

Quenching from different temperatures followed by metallography and microscopy was used to study the transformation temperatures based on the microstructural changes. In total 16 different temperatures for solution treatment were selected: 600, 690, 752, 763, 790, 800, 808, 826, 846,

864, 876, 895, 904, 916, 930 and 968°C. Detail of heating and quenching procedures can be found in [14].

2.2 Mechanical and Creep tests

The effect of aging treatments on mechanical responses was assessed using Vickers hardness test. Hardness of the samples was measured on the axial-radial cross-section of the tube employing a Buehler Macro-Vickers 5100 hardness testing machine to apply a 10kg load; for each sample, hardness was measured at least at five different locations and the average result is reported. Room temperature uniaxial tensile tests were subsequently carried out on two microstructures: 1) water-quenched from 890°C, 2) water-quenched from 890°C then aged at 450°C for 1 hour. The samples were strained at a constant crosshead speed of 0.001 $mm.s^{-1}$ equivalent to a nominal strain rate of about $10^{-4}s^{-1}$; details of test specimen geometry and preparation are provided in [14]. Furthermore, high temperature tensile tests at 400°C were carried out on the following samples: heat treated at 890°C and water-quenched followed by aging at 450°C for 1 hrl; heat treated at 890°C and air-cooled followed by stress relieving at 450°C for 1 hr; heat treated at 980°C and water-quenched followed by aging at 450°C for 1 hr; as-received Excel. For stress-rupture tests, the above mentioned samples were first heated to 400°C using an infrared heater keeping a constant pre-load of about 50N on the sample (a stress of approximately 6MPa). After reaching the temperature the load was increased to the predefined constant value (80-92% UTS at 400°C) at a constant rate of 4 N/s (approximately 0.5MPa/s), at which load the sample was held until fracture. Strain measurement during the test was accomplished by digital image correlation. Both high temperature tensile tests and stress-rupture tests were carried out on the samples taken from both the axial and transverse directions of the pressure tube.

2.3 In-Situ Irradiation experiments

A series of in-situ irradiation experiments on various Excel microstructures investigated microstructural evolution. The work concentrated on the formation of <c>-loop nucleation, their growth, the stability of the β-phase under irradiation and the effect of pre-existing microstructure. In-situ experiments were carried out at the IVEM-Tandem Facility at Argonne National Laboratory. The Facility includes a Hitachi H-9000NAR transmission electron microscope interfaced with a 2MV tandem ion accelerator. TEM samples from HT material were mounted in a double-tilt heating holder and irradiated at 400, 300, or 100°C with 1 MeV Kr2+ ions to maximum total doses ranging from 1 to 10 dpa. Equipment and experimental details are provided in [15].

3 Results and discussion

3.1 Microstructural characterization

Selected TEM micrographs after various heat treatments are shown in Figure 1, with heating and quenching carried out at 600-970°C. Manual point counting on SEM micrographs was employed to determine the transformation temperatures of Excel alloy. The $\alpha_{Zr} \rightarrow \alpha_{Zr}+\beta_{Zr}$ transformation temperature, i.e. the temperature at which the volume fraction of stabilized β_{Zr} starts to increase was found to be between 600-690°C corresponding to an increase in the volume fraction of β_{Zr} from 13% to 19%. The $\alpha_{Zr}+\beta_{Zr} \rightarrow \beta_{Zr}$ transus temperature was found to be approximately 968°C at which the microstructure after quenching is almost fully martensitic except some few isolated

small α_{Zr} grains. It was found that by increasing the solution treatment temperature, the volume fraction of β_{Zr} or transformed β_{Zr} increases until at 968°C the microstructure is fully transformed β_{Zr}, i.e. fully martensitic. The volume fraction of β_{Zr} as a function of temperature is presented in Figure 2; the rapid increase in the β_{Zr} volume fraction at 864°C corresponds to β_{Zr} fully transformed to α′ martensite. Below 864°C, the β_{Zr} does not fully transform to martensite and remains untransformed with only a few martensite laths inside the β_{Zr} grains. This is due to the fact that at these temperatures the concentration of β_{Zr}-stabilizing elements, i.e. Mo and Nb is high enough to suppress the α′-martensite-start temperature, Ms, to ambient temperatures. Instead, the β_{Zr} microstructure transforms into a mixture of athermal hexagonal (P6/mmm) ω and α″-martensite in a matrix of β_{Zr}.

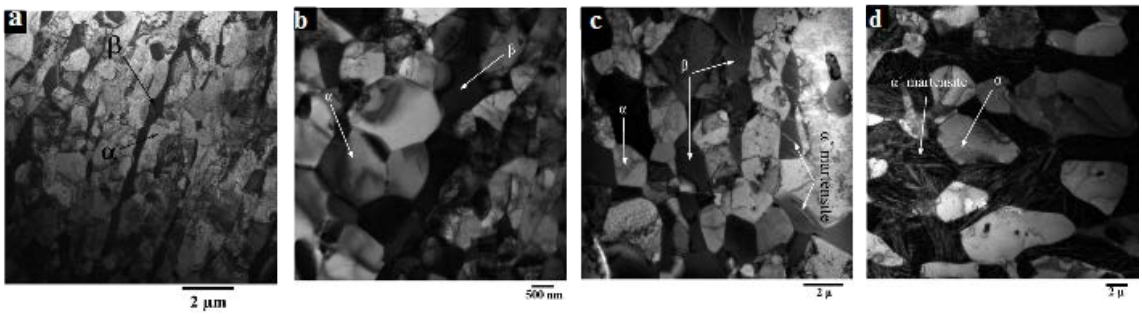

Figure 1. TEM micrographs of a) as received, and water quenched samples after 2 hours solution treatment at b) 690°C, c) 800°C, d) 876°C.

Figure 3 shows the microstructure of the three different solution treatments namely: solution treated at 890°C followed by water-quenching, 980°C followed by water-quenching and 890°C followed by air-cooling. At 980°C the microstructure is fully β-bcc which transforms into α′ -hcp martensite upon quenching.

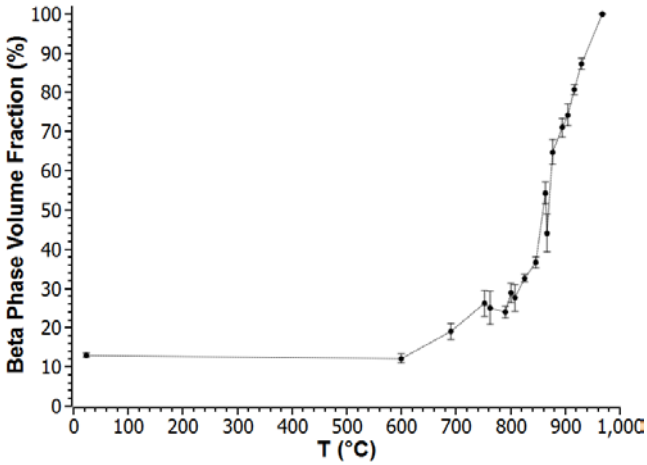

Figure 2. Volume fraction of beta-phase (%) as a function of temperature from which the samples were quenched.

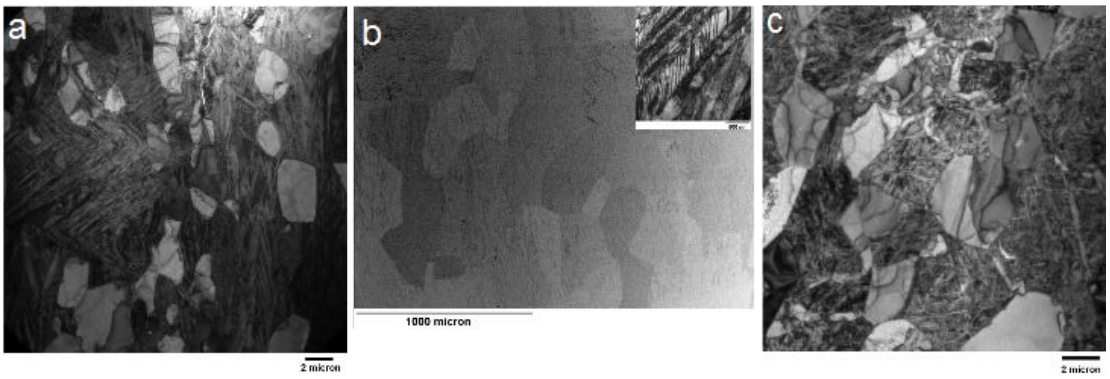

Figure 3 a) TEM micrograph of the sample water-quenched from 890°C. b) SEM and TEM (inset) micrograph of the sample water-quenched from 980°C. c) TEM micrograph of the sample air-cooled from 890°C.

The temperature 890°C lies in the α+β region with α and β-phases having an approximate volume fraction of 29% and 71% respectively. Upon quenching, the β-phase transforms into α′-hcp martensite while the α-phase remains unchanged. Solution treating at 890°C and water-quenching followed by aging at 450°C for 1 hour produces Mo and Nb rich precipitates in the martensitic phase; however no precipitation occurs in the α-phase. Solution treated Excel at 890°C followed by air-cooling to room temperature and stress relieving at 450°C for 1 hour results in the transformation of the β-phase into a combination of fine Widmanstätten α-hcp grains with a continuous network of β-bcc along the grain boundaries. There is no precipitation as a result of the heat treatment at 450°C. Solution treating at 980°C and water-quenching followed by aging at 450°C for 1 hour results in a fully martensitic microstructure with Mo and Nb rich precipitates in the martensitic phase as in the case of the sample water-quenched from 890°C.

3.2 Creep and mechanical behaviour

High temperature tensile test at 400°C were performed on the developed microstructures in both axial and transverse directions as shown in Figure 4. From the tensile tests, it is evident that the water-quenched microstructures have high strength and low ductility while the air-cooled microstructure exhibited higher strength and comparable ductility as compared to the cold-worked and annealed microstructure. The 400°C tensile test results showed very high strength for the martensitic microstructure, i.e. UTS of 892-917 MPa and 815-832 MPa for the samples water-quenched from 980°C and 890°C and aged, respectively. However, the total elongation was quite low in the range of 3% and 6-12% for the above microstructures, respectively.

The air-cooled sample with Widmanstätten microstructure showed relatively higher tensile strength compared to the as-received material but with comparable ductility. The results of 400°C tensile tests show a predictable trend for the investigated microstructures. The yield stress and tensile strength increase in order from as-received to 890°C air-cooled with equiaxed α and Widmanstätten microstructure, to 890°C water-quenched with equiaxed α and precipitation hardened martensite microstructure, and finally 980°C water-quenched with precipitation hardened fully martensitic microstructure. The ductility decreases in the same order, with the strain at fracture of the 890°C air-cooled sample (21.2%) being slightly higher than the as-received sample (19.3%) in the transverse direction. The anisotropy in mechanical properties, i.e.

the difference between transverse and axial direction, becomes less in the same sequence of microstructures; for the 980°C water-quenched sample the yield stress in the axial and transverse directions are almost the same and the tensile strength in the axial direction is slightly higher than in the transverse direction. This is a result of change in the texture due to the different heat treatments.

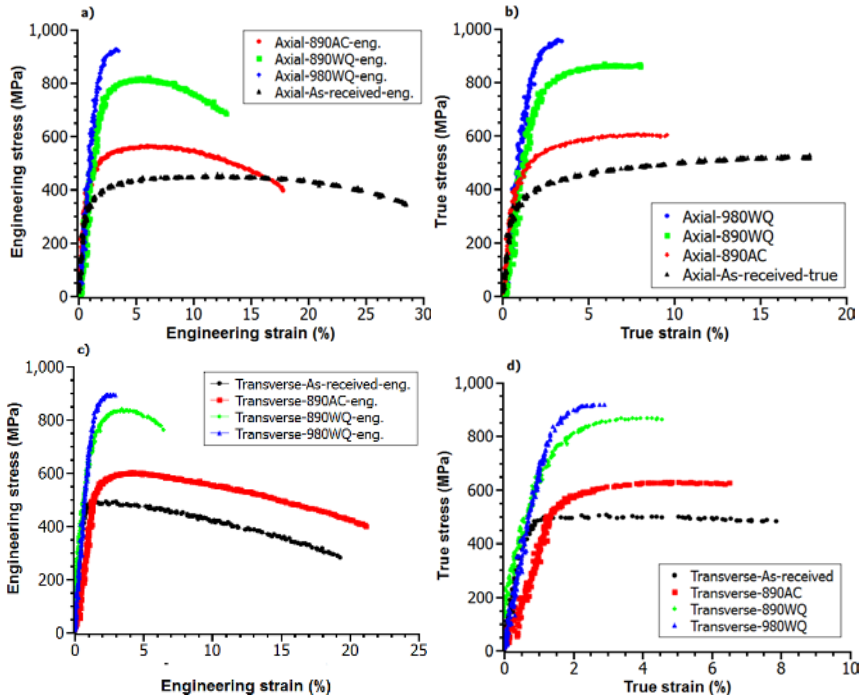

Figure 4. 400°C engineering and true stress-strain curves for the as-received, 890°C air-cooled, 890°C water-quenched, and 980°C water-quenched microstructures. a) and b) axial, c) and d) transverse directions (All the samples aged at 450°C for 1 hr)

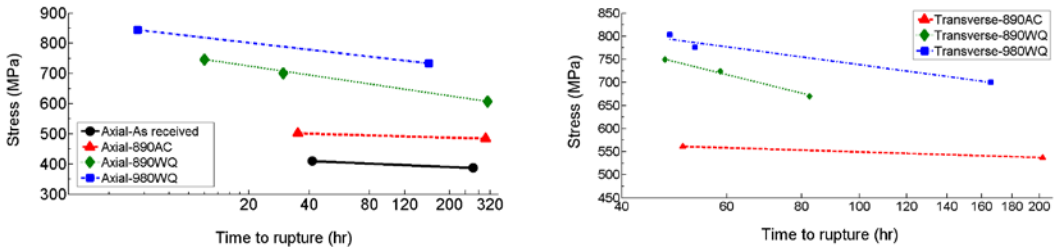

Figure 5. Creep-rupture graphs of Excel pressure tube material with different heat treatments in the axial (left) and transverse (right) directions

If we consider potential applications of the Excel alloy as a pressure tube material in the CANDU-SCWR, the air-cooled Widmanstätten microstructure seems to be the most promising microstructure, with a combination of relatively high strength, high ductility and low creep rate. The 400°C yield stress of this microstructure in the axial and the transverse directions (420MPa and 555 MPa, respectively) are about 2.8 times and 1.8 times the design stress, respectively (150 MPa and 300 MPa). However, the fully martensitic and aged microstructure shows low creep rates at higher stress levels, thus at the same stress level with the air-cooled microstructure it might show even lower creep rates. Therefore, it should not be ruled out merely based on its low

ductility. The observed increase in strength of the heat treated samples is consistent with predictions based on Hall-Petch and Orowan looping mechanisms.

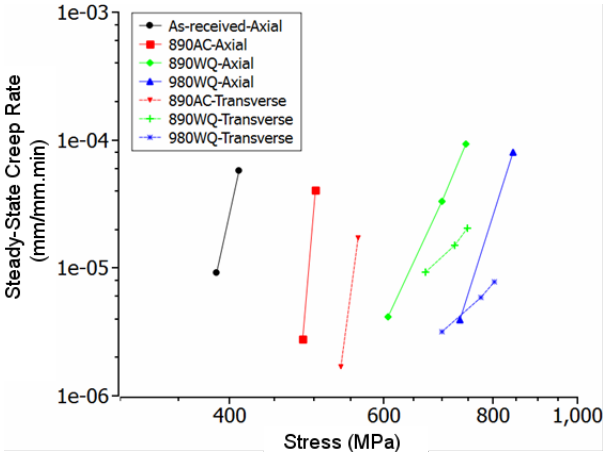

Figure 6. Log-log plot of steady-state creep rates vs. stress for different microstructures.

High temperature creep-rupture experiments were performed at 400°C on the developed microstructures as shown in Figure 5. The creep-rupture results and the stead-state creep rates in the axial and transverse directions (Figure 6) reveal that of all the microstructures the 980°C water-quenched and 890°C air-cooled have better creep properties at high stresses and relatively low stresses respectively. The creep-rupture tests showed that 980°C water-quenched and 890°C air-cooled samples had the lowest creep rates. Note that the creep rates of the 980°C water-quenched sample were comparable to the 890°C air-cooled samples despite the fact that the stress levels were significantly beyond the UTS of the 890°C air-cooled samples. The stress exponent for all the samples were high, in the power law breakdown region except for the samples water-quenched from 890°C and 980°C which were in the range of power law creep [16].

4 Irradiation induced microstructural changes

4.1 Formation of <c>-component loops in alpha phase

Selected microstructures from the heat treatment experiments discussed above were studied under an irradiation environment. Microstructures were: i) water quench from 855^{o}C, ii) water quench from 890^{o}C then age for one hour at 450^{o}C (WQ samples), iii) water quench from 890^{o}C, then aged for 550 hours at 500^{o}C (OA samples). The latter produced large (~20-100 nm) $Zr_3(Mo,Nb,Fe)_4$ precipitates in α-phase with a hexagonal crystal structure.

From in-situ irradiation of 890^{o}C WQ and aged for one hour at 450^{o}C, it was found that formation of <c>-component loops in α-phase occurs at 400, 300 and 100^{o}C after a threshold incubation dose, shown in Figure 9. The threshold incubation dose is both temperature and initial microstructure dependent; it increases with a decrease of temperature (Figure 9). Threshold incubation dose for the formation of <c>-component loops increases in the similar microstructure after aging for 550 hours at 500^{o}C (OA samples) (see Figure 8). This phenomenon can be attributed to radiation induced dissolution and re-distribution of alloying elements from secondary phase precipitates (SPP), which occur readily at higher temperature

(400°C) as compared to lower temperatures (300 and 100°C); this was confirmed by EDS mapping (Figure 9).

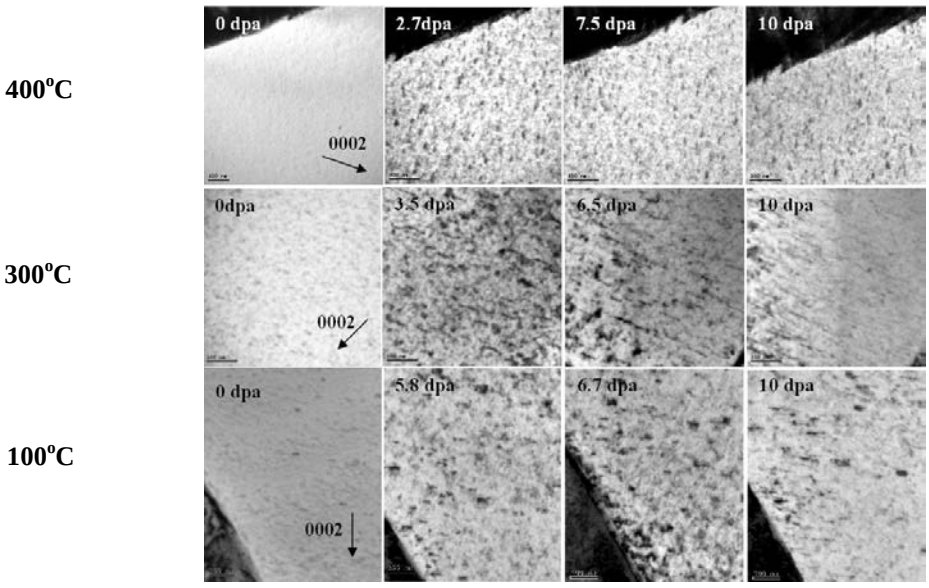

Figure 7. Formation of <c>-component loops in 890°C water quenched then aged for one hour at 450°C.

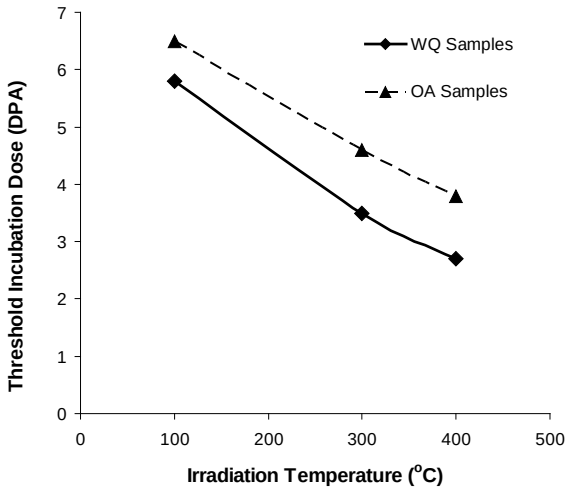

Figure 8.Variation in threshold incubation dose for the formation of <c>-component loops as a function of irradiation temperature (890°C-water quenched-aged for one hour at 450°C (WQ) and 890°C-water quenched-aged for 550 hour at 500°C (OA)).

From EDS mapping, the formation of <c>-component (Figure 9) loops can be related to the presence of Fe in the α-phase which is dissolved and redistributed from SPP into the α-phase. The presence of alloying elements in α-phase results in the decrease of stacking fault energy which assists the formation of <c>-component loops [8]. A further decrease in threshold incubation dose was seen in OA samples, due to the presence of SPP. This is because a higher dose is required to dissolve the SPP and redistribute the elements. Figure 7 shows the formation of <c>-loops in the sample solution treated at 855°C-WQ. The effect of cascade damage on the re-distribution of alloying elements from SPP has been shown in Figure 8.

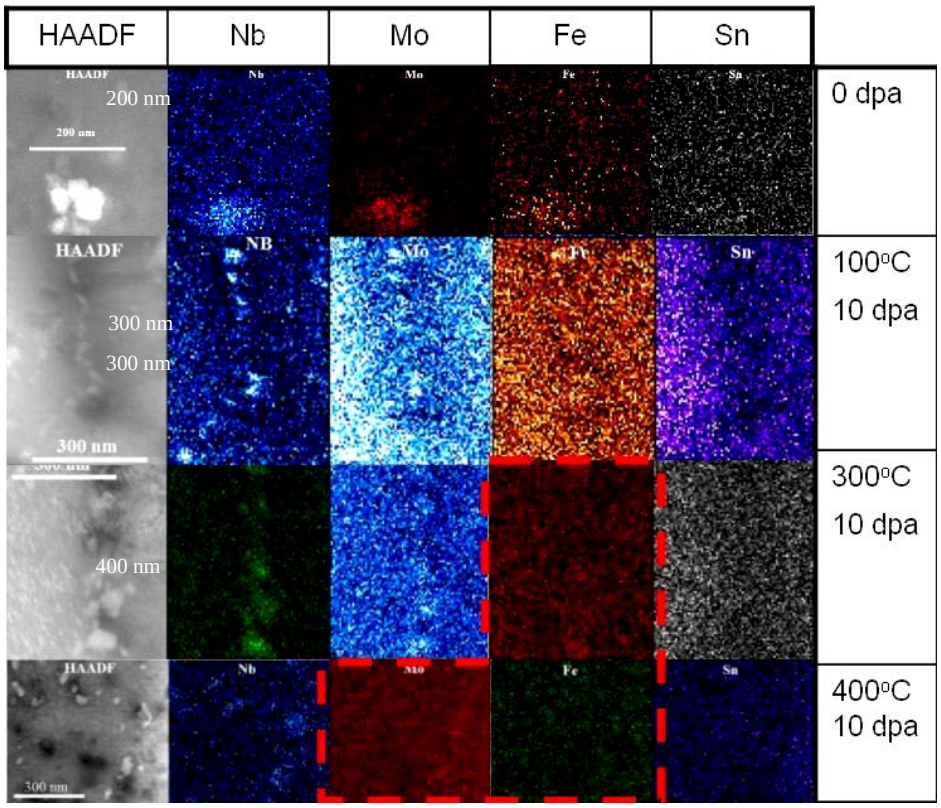

Figure 9. Effect of radiation damage on Mo-Nb-Fe rich SPPs. Fe leaves SPP into α-phase at all irradiation temperature.

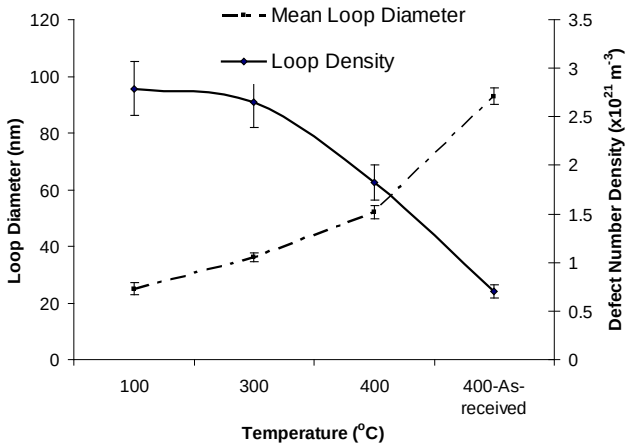

Figure 10. <c>-component loop size and density after 10 dpa as a function of temperature in as received and 855°C-WQ samples.

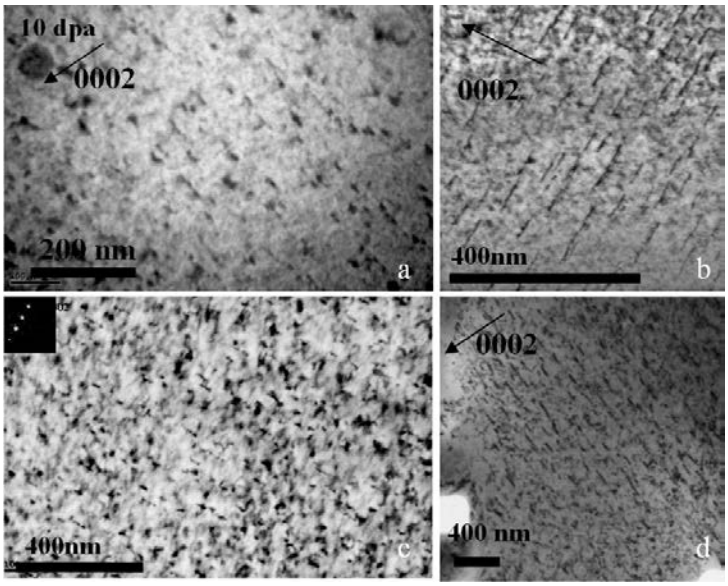

Figure 11. TEM micrographs showing the formation of <c>-loops in samples water quenched from 855°C, at a. 400, b. 300 and c. 100°C, d. 400°C in as-received sample.

The morphology and density of <c>-component loops is found to be temperature and dose dependent (Figure 11). The loop size increases whereas the loop density decreases with an increase of irradiation temperature as shown in Figure 10. Furthermore, it has been observed that the loop density in as-received Excel is lower, and loop size is higher as compared to the sample heat treated at 855°C, as shown in Figure 10.

4.2 Irradiation induced decomposition of beta phase

The behaviour of the β-phase under irradiation has been studied by irradiating the samples after a solution treatment at 855°C for two hours, followed by water quenching. Very small ω-phase particles are formed during the quenching. After the irradiation to 10 dpa at 400, 300 and 100°C, it is found that the β-phase is further decomposed into larger ω-phase precipitates under irradiation as shown in Figure 12. The size distribution of ω-phase as a function of dose and temperature is shown in Figure 13. However, it should be noted that ω-phase precipitation is seen to occur during aging experiments in unirradiated samples as well. This isothermal ω-phase has a different morphology than irradiation induced ω-phase. It is evident from Figure 13 that the volume fraction of isothermal ω-phase increases with temperature. We see isothermal ω-phase precipitates grow during aging at and above 300°C. However in the case of radiation damage, there is a process of dissolution (or disordering) of ω-phase due to the atomic displacement within the collision cascades [17], which is in competition with the irradiation induced nucleation process. Irradiation causes an increase in the free energy of the β-phase by generating a high concentration of point defects, making it more unstable and causing a transformation from β-phase to ω-phase. β-phase undergoes thermal decomposition which may be arrested or reversed by irradiation [18]. Destruction, nucleation and growth of ω-phase occurs at the same time during the irradiation experiments, however the growth of β-phase occurs once the rate of nucleation is higher than the rate of dissolution, to achieve the new equilibrium conditions.

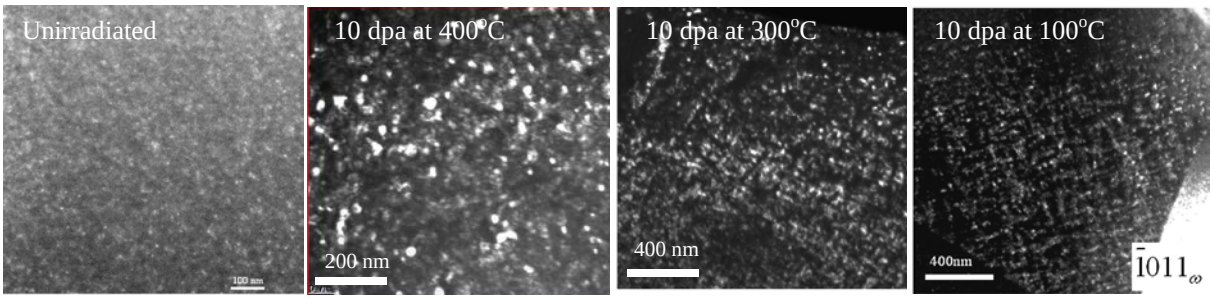

Figure 12. Formation of irradiation induced ω-phase within pre-existing β-phase of samples water quenched from 855°C at 400, 300 and 100°C.

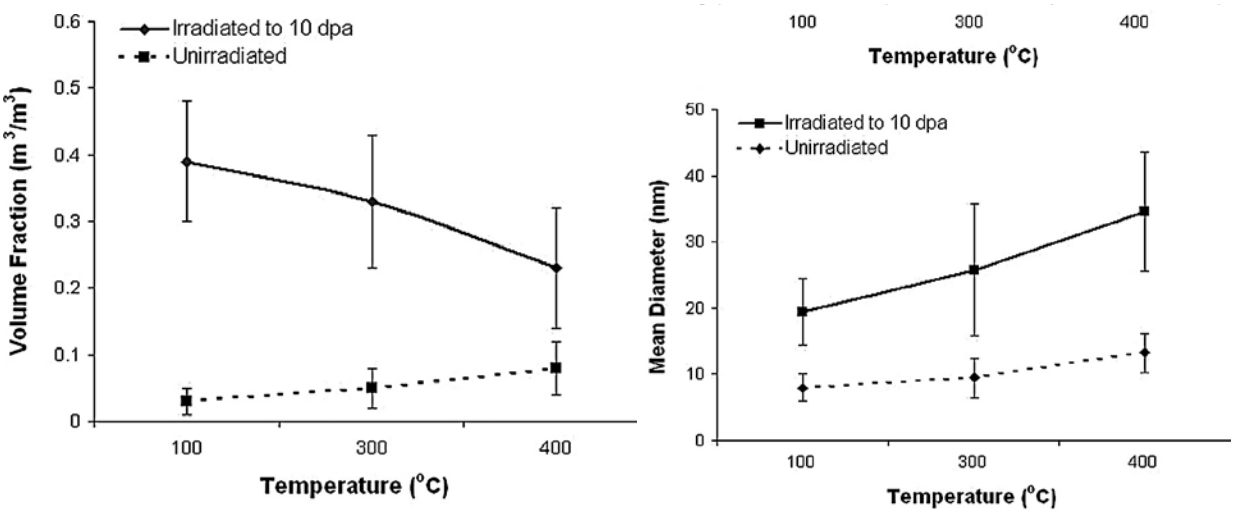

Figure 13. Volume fraction and mean diameter of irradiation induced (10 dpa) and isothermal ω-phase as a function of irradiation temperature, in sample 855°C-WQ.

5 Summary and conclusions

1- The water-quenched microstructures showed very high strength and low ductility while the air-cooled microstructure exhibited higher strength and comparable ductility to the cold-worked and annealed (i.e. as-received) microstructure.
2- The creep-rupture results and the secondary creep rates showed that among all the microstructures, the 980°C water-quenched and 890°C air-cooled have better creep properties at high stresses and relatively low stresses respectively.
3- <c>-component loops nucleate and grow at 400, 300 and 100°C after a threshold incubation dose which is dependent on both temperature and parent microstructure.
4- β-phase decomposed into irradiation induced ω-phase in the form of large precipitates.

6 References

[1] T. Reiss, G. Csom, S. Fehér, S. Czifrus, Prog. Nucl. Energy., 52 (2010) 177-189.
[2] C.K. Chow, H.F. Khartabil, Nucl. Eng. Tech., 40(2) (2008)139-146.
[3] C.D. Williams, C.E. Ells, P.R. Dixon, Canadian Metallurgical Quarterly 11 (1972) 257-271.

[4] E.F. Ibrahim, B.A. Cheadle, Canadian Metallurgical Quarterly 24 (1985) 273-281.
[5] E.F. Ibrahim, E.G. Price, A.G. Wysiekiersky, Can. Metal. Quart., 11 (1972) 273-283.
[6] B.A. Cheadle, R.A. Holt, V. Fidleris, A.R. Causey, V.F. Urbanic, Zirconium in the Nuclear Industry, Fifth International Symposium, ASTM STP., 754(1982) 193-207.
[7] A.R. Causey, G.J.C. Carpenter, S.R. MacEwen, J. Nucl. Mater., 90 (1980) 216-223.
[8] M. Griffiths, J. Nucl. Mater., 159 (1988) 190-218.
[9] R. Tucker, V. Fidleris, R.B. Adamson, ASTM STP., 824(1984) 427-451.
[10] A. Jostsons, P.M. Kelly and R.G. Blake, ASTM STP., 683 (1978) 46.
[11] D.O. Northwood, R.W. Gilbert, L.E. Bahen, P.M. Kelly, R.G. Blake, A. Jostsons, P.K. Madden, D. Faulkner, W. Bell, R.B. Adamson, J. Nucl. Mater., 79 (1979) 379-394.
[12] M. Griffiths, M.H. Loretto, R.E. Smallman, J. Nucl. Mater., 115 (1983) 313-322.
[13] Y. Idrees, Z. Yao, M. Sattari, M.A. Kirk, M.R. Daymond, J. Nucl. Mater., 441 (2013) 138–151.
[14] M. Sattari, R.A. Holt, M.R. Daymond, Journal of Nuclear Materials 435 (2013) 241-249.
[15] Y. Idrees, PhD Thesis, Queens University (2013).
[16] M. Sattari, PhD Thesis, Queens University (2012).
[17] R.S. Nelson, J.A. Hudson, D.J. Mazey, J. Nucl. Mater. 44 (1972) 318–330.
[18] M. Griffiths, J.F. Mecke, J.E. Winegar, ASTM STP 1295 (1996) 580–602.